SAND2017-2193J

Flame Thickness and Conditional Scalar Dissipation Rate in a Premixed Temporal Turbulent Reacting Jet

Swetaprovo Chaudhuri[1,*], Hemanth Kolla[2,*], Himanshu L. Dave[1,*], Evatt R. Hawkes[3], Jacqueline H. Chen[2,**], Chung K. Law[4]

[1]Department of Aerospace Engineering, Indian Institute of Science, Bangalore 560012, India

[2]Combustion Research Facility, Sandia National Laboratories, Livermore, CA 94551, USA

[3]School of Mechanical and Manufacturing Engineering / School of Photovoltaic and Renewable Energy Engineering, The University of New South Wales, Sydney, NSW 2052, Australia

[4]Department of Mechanical and Aerospace Engineering, Princeton University, Princeton, NJ 08544, USA

Abstract: The flame structure corresponding to lean hydrogen-air premixed flames in intense sheared turbulence in the thin reaction zone regime is quantified from flame thickness and conditional scalar dissipation rate statistics, obtained from recent direct numerical simulation data of premixed temporally-evolving turbulent slot jet flames [1]. It is found that, on average, these sheared turbulent flames are thinner than their corresponding planar laminar flames. Extensive analysis is performed to identify the reason for this counter-intuitive thinning effect. The factors controlling the flame thickness are analyzed through two different routes *i.e.*, the kinematic route, and the transport and chemical kinetics route. The kinematic route is examined by comparing the statistics of the normal strain rate due to fluid motion with the statistics of the normal strain rate due to varying flame displacement speed or self-propagation. It is found that while the fluid normal straining is positive and tends to separate iso-scalar surfaces, the dominating normal strain rate due to self-propagation is negative and tends to bring the iso-scalar surfaces closer resulting in overall thinning of the flame. The transport and chemical kinetics route is examined by studying the non-unity Lewis number effect on the premixed flames. The effects from the kinematic route are found to couple with the transport and chemical kinetics route. In addition, the intermittency of the conditional scalar dissipation rate is also examined. It is found to exhibit a unique non-monotonicity of the exponent of the stretched exponential function, conventionally used to describe probability density function tails of such variables. The non-monotonicity is attributed to

[*]These authors contributed equally to this work
[**]Corresponding Author, Email: jhchen@sandia.gov

the detailed chemical structure of hydrogen-air flames in which heat release occurs close to the unburnt reactants at near free-stream temperatures.

Keywords: Direct numerical simulations; Detailed chemistry; Flame thickness; Conditional scalar dissipation rate; Probability density functions

1. Introduction

Scalar dissipation rate (SDR) is a central quantity in both non-reacting and reacting turbulent flows involving scalar transport. It denotes the rate at which large scale inhomogeneity of the scalar field is broken down into smaller scales under the straining action of turbulence, and is eventually dissipated by molecular diffusion. Hence, scalar mixing in a turbulent flow is characterized by SDR. In reacting flows, the interpretation of SDR becomes richer. For non-premixed turbulent flames where the fuel and oxidizer must be mixed at the molecular level to sustain reactions, Peters [2] identified SDR as the inverse of the characteristic diffusion time scale. The connections between the mean reaction rate and the scalar dissipation rate have been utilized and derived in [3, 4] and [5-7], respectively. Thereafter, the mean scalar dissipation rate of the progress variable [8], the mean dissipation rate of a level set variable [9], or a functional of the scalar dissipation rate spectrum of a level set variable [10] have been shown to be related to the turbulent flame speed. For premixed combustion, one can connect the conditional scalar dissipation rate (CSDR) to the local flame thickness. CSDR is defined as the square of the magnitude of the gradient of a scalar; the flame thickness can be defined proportional to the inverse of the magnitude of the scalar gradient. The flame thickness is the width over which the entirety of the chemical to thermal energy conversion occurs, and thus the distribution of this quantity is of fundamental importance. Flame thickness is also an important parameter in the definition of regime diagrams of premixed turbulent combustion.

In a premixed flame, a strong scalar gradient spanning over the flame thickness separates the unburnt cold reactants from the hot burnt products. On interaction with turbulence, the flame shape and local structure may be modified and turbulence may either lead to production of the scalar gradient or its dissipation depending upon the Damköhler number (Da) and the Karlovitz number (Ka) among other parameters. If the scalar is passive without any source to support the gradient, the ultimate state would be a homogeneous mixture at the end of the collective stretching and diffusion processes. But for premixed flames the heat release sustains the gradient and also tends

to destroy the local turbulent strain due to dilatation. The dilatation of fluid volume in regions of substantial heat release within the flame can strongly alter the eigenvalues (*i.e.* principal strains) and the alignment of the eigenvectors of the fluid deformation rate tensor (S_{ij}) with respect to the scalar gradient (or local normal) [11]. This has a profound effect on the scalar gradient production or dissipation. Hence, it is of interest to understand how turbulence and heat release compete to define the scalar gradient, and consequently the flame thickness and SDR. Fundamental understanding of the turbulence-scalar interaction gleaned from the statistics of SDR or CSDR and flame thickness can also aid in turbulent flame modeling [11-13].

It must be recognized that while fluid strain rates are ubiquitous and well understood, additional strain rates exist in the premixed flames due to the change in the flame displacement speed (S_d). For example, in a standard, steady one-dimensional laminar premixed flame S_d monotonically increases from unburnt to burnt region, just like the fluid velocity, due to the density decrease. While the increase in the fluid velocity induces a positive fluid normal strain rate (a_N) trying to separate two iso-scalar surfaces, the increase in the flame displacement speed induces a negative strain rate along the local normal direction and tends to bring the two iso-scalar surfaces closer. These two strain rates balance each other in this planar, laminar, unstretched, premixed flame, resulting in a constant flame thickness. The behavior of these strain rates in a turbulent premixed flame, however, may vary in a more complicated manner. The statistics of these two strain rates in a shear driven turbulent reacting flow with non-unity Lewis number effects and their consequent role in controlling the flame thickness and SDR are extensively studied and discussed in the present study.

One of the hallmarks of passive scalar turbulence is that, similar to the energy dissipation rate, the scalar dissipation rate is also a highly intermittent quantity. Intermittency in the fields is characterized by instantaneous values which may deviate significantly from the corresponding mean values. In the probability density function (pdf) description, the probability of occurrence of such extreme events is higher compared to the measures from the Gaussian distribution. In addition, these extreme values are randomly distributed in time or space. Intermittency of the scalar dissipation rate of passive scalars is a major topic in turbulence research which has received extensive attention over the decades. For reactive scalars, though the importance of intermittency has been recognized [14], it has seldom been addressed in the context of turbulent premixed flames except for its introduction in models [15, 16] and recently in [17].

The paper is organized as follows. The next section briefly introduces the datasets obtained from the direct numerical simulation (DNS) of temporally evolving jet. Section-3 defines the slightly modified definition of flame thickness and SDR used in this paper. Section-4 presents the results and discussions on the pdfs of normalized flame thickness and CSDR; the statistics of the strain rates discussed above; the effect of mean shear; the intermittency of the CSDR and its implications along with some few additional important points. The final section concludes with the findings of this study.

2. DNS of lean hydrogen-air premixed temporally-evolving slot jet flame

Statistics related to the pdfs of flame thickness and CSDR were obtained from a recent petascale DNS of lean hydrogen-air combustion with detailed chemistry in a temporally evolving slot-jet configuration [1]. In this configuration, two initially planar lean hydrogen-air premixed flames at an equivalence ratio of $\phi = 0.7$ and unburnt temperature of 700K propagate towards each other, crossing through a plane turbulent jet of unburnt premixed reactants. Spatio-temporal scales down to the mean Kolmogorov length scales and time scales were resolved in the simulation. The H_2-air chemistry was modeled by the detailed chemical reaction mechanism of [18]. DNS of turbulent premixed flames has been performed predominantly in the absence of mean shear with the exception of a few studies [19], [20]. Mean shear contributes to turbulence production, which enhances its interaction with the flame. In the absence of mean shear, heat release can dissipate turbulence within the flame, targeting particularly the fine scales. In [19], the spatial resolution was not fine enough to study small-scale interactions quantitatively, and in [20], the DNS was performed with simple chemistry and at low Reynolds numbers. Hence, the coupling between mean strain, turbulent strain, and mixing and reaction is still not well understood.

Two cases are considered with different Damköhler numbers ($Da = l_T S_L / u'' \delta^*_{L,Lam}$: where l_T is the integral length scale; S_L the unperturbed planar laminar flame speed; u'' the r.m.s. of fluctuating velocity and $\delta^*_{L,Lam}$ the unperturbed planar laminar flame thickness), henceforth referred to as *Da*- and *Da*+ for the smaller and larger Damköhler numbers, respectively, while the Reynolds number is held fixed. *Da*+ is greater than unity while *Da*- is less than unity throughout the simulation as the turbulence-flame interaction develops in time. The turbulent jet Reynolds number is: $Re_{jet} = UH/\nu_0 \sim 10000$; where H is the slot jet height, U the peak mean jet velocity,

and ν_0 the kinematic viscosity of the unburned reactants. The turbulence Reynolds number is: $Re_t = u'' l_T/\tilde{\nu} \sim 1000$; here $\tilde{\nu}$ is the Favre averaged kinematic viscosity. The number of grid points across $\delta^*_{L,Lam}$ is 14 for the *Da+* case, while the *Da-* case has nearly twice the resolution of the *Da+* case. Other relevant simulation parameters are given in Table 1. The turbulent kinetic energy spectra exhibit Kolmogorov's $k^{-5/3}$ scaling over a decade of inertial range scales. In the temporal configuration, time-dependent statistics are obtained by averaging in the homogeneous streamwise and spanwise directions. In the present study, statistics are presented mostly at a normalized jet time, $t/t_j = 15$, corresponding to a time in the DNS with significant turbulence-flame interaction. Here the jet time is defined as $t_j = H/U$ at this particular instant in time; the flames at both *Da-* and *Da+* conditions are well developed (as can be verified from their near peak turbulent flame speeds, see Fig. 9 in [1]) and they have propagated into the strong shear region of the jet.

Table 1: Simulation parameters reproduced from [1]

Parameter	Case *Da-*	Case *Da+*
$\boldsymbol{Da_{jet}}$	0.13	0.54
$\boldsymbol{H}$ (mm)	2.7	5.4
$\boldsymbol{U}$ (m/s)	312.6	156.3
$\boldsymbol{dx}$ (mm)	18	36
$\boldsymbol{dt}$ (ns)	2.5	5

The evolution of the turbulence and flame conditions pertaining to the *Da-* and *Da+* cases are shown in the turbulent premixed combustion regime diagrams of Fig. 1(a). Snapshots of the iso-scalar surfaces of the maximum heat release rate for these two cases at $t/t_j = 15$ are shown in Figs. 1(b) and 1(c), respectively. During the simulations, Re_t peaks at 810 with $Ka = 92$ for the *Da-* case. For the *Da+* case, the peak is $Re_t = 960$ with corresponding $Ka = 22$. Further details of the configuration and numerical techniques are given in [1]. The results and insights gleaned from the present study may be practically useful, given that most practical flames encountered either in the swirling flow of a gas turbine combustor or in the wake of a bluff body separated flow of an afterburner are stabilized and stretched by the straining action of a turbulent shear layer.

3. Definition of flame thickness and CSDR

For a unperturbed planar laminar premixed flame, the thermal thickness is often defined as [21]:

$$\delta^*_{L,Lam} = (T_b - T_u)/|\boldsymbol{\nabla} T|_{max} \quad (1)$$

where T denotes temperature, while subscripts u and b corresponding to the unburnt and burnt side. $|\boldsymbol{\nabla} T|_{max}$ is the maximum of magnitude of the temperature gradient. This definition is frequently used to determine the preheat zone thickness in turbulent premixed flames as well, [22]. Here, we consider a slightly different definition, based on temperature gradient measurements at different isothermal surfaces within the premixed flame structure. The definition of thermal flame thickness that is used henceforth, unless otherwise specified, is given by:

$$\delta_L = (T_b - T_u)/|\boldsymbol{\nabla} T|_{T=T_0} \quad (2)$$

The subscript $T = T_0$ implies that the gradient is measured at an isothermal surface with $T = T_0$. The scalar dissipation rate based on temperature is defined as $\chi = \alpha(\boldsymbol{\nabla} T . \boldsymbol{\nabla} T)$, where α is the thermal diffusivity which is predominantly a function of temperature. Thus, if χ is measured on an isothermal surface; α is essentially a constant and could be omitted for simplicity. Thus, in this paper we define CSDR as:

$$\chi_{T_0} = \boldsymbol{\nabla} T . \boldsymbol{\nabla} T|_{T=T_0} \quad (3)$$

The flame thickness definition given by eq. (2) is more tractable in terms of analysis, and its connection to conditional scalar dissipation rate (CSDR) that describes turbulence-scalar interaction is more apparent.

To keep our results independent of choice of the scalar we will focus on the distribution of δ_L and CSDR conditioned on progress variable. Initially, the progress variable is defined as $c = (T - T_u)/(T_b - T_u)$. In the supplementary material (section S.1) we have also explored the pdfs based on an alternative definition of the progress variable defined as $c_{Y_{O_2}} = \left(Y_{O_2} - Y_{O_{2,u}}\right)/\left(Y_{O_{2,b}} - Y_{O_{2,u}}\right)$ where Y_{O_2} is the mass-fraction of O_2. Figure 2 explores the relationship between c and $c_{Y_{O_2}}$ for a planar laminar premixed flame, which shows significant deviation from linearity. This suggests that progressing across the flame, even with a moderate temperature rise, most of the O_2 has been consumed.

In the thin reaction zones regime, the preheat layer of the flame may be perturbed, and if so, it may be inappropriate to extrapolate the "gradient" based thickness definition, eq. (2), from laminar to turbulent flames in this regime. Hence, we also investigate a "geometric" definition of the flame thickness, which is based on the minimum distance between two iso-scalar surfaces. The geometric flame thickness at a point $(x_0, y_0, z_0) \in c = c_0$ with respect to another iso-scalar surface $c = c_1$ is given by:

$$\delta_{L,geom}(x_0, y_0, z_0) = min\sqrt{(x - x_0)^2 + (y - y_0)^2 + (z - z_0)^2} \quad (4)$$

for all $(x, y, z) \in c = c_1$. Scanning over all $(x_0, y_0, z_0) \in c = c_0$ a flame thickness pdf can be constructed.

4. Results and discussions

This section is sub-divided into five sub-sections, each addressing specific aspects. First, we explore the variation of the pdfs of the logarithm of δ_L with increasing values of the progress variable. The following sub-section discusses the pdfs of the logarithm of CSDR. Discussions on the effect of mean shear, pdfs of alignment of eigenvectors of S_{ij} with local normal, and the intermittency of CSDR are then presented. The motivation for looking into the pdfs of logarithmic variables is the following. It is known that the SDR for a passive scalar exhibits near lognormal behavior with some negative skewness. For non-reacting flows, this has been shown by both experiments [23] and DNS [24]. For non-premixed turbulent combustion, such near lognormality of SDR was demonstrated experimentally in [25] and computationally in [26] and [27]. Discussion on the pdf shape of the SDR or CSDR for turbulent premixed flames is rare with the exception of [17], in which the connection between flame thickness and CSDR was discussed alongside a demonstration of their near lognormality and the deviation from the same. If the CSDR is lognormally distributed in the present study of reactive scalars as well, then the flame thickness, eq. (2), must also be lognormally distributed, since by definition, $\delta_L \sim \chi_{T_0}^{-1/2}$. The assumption that χ_{T_0} is a lognormal variable implies that $\ln(\chi_{T_0})$ has a normal distribution. Hence any exponent on χ_{T_0} appears as a constant factor ahead of $\ln(\chi_{T_0})$, thus rendering δ_L a lognormal variable.

4.1 Pdfs for flame thickness

In Figs. 3(a) and 3(b), the pdfs of the natural logarithm of the normalized flame thickness: $\delta_L/\delta_{L,Lam}$ at different progress variable iso-levels: $c = c_0$, for $c_0 = 0.01$ and 0.1 to 0.9 in increments of 0.1 are plotted, where $\delta_{L,Lam}$ is the flame thickness calculated using eq. (2) obtained from unperturbed laminar flame simulations using the PREMIX code [28]. To understand the effect of strained laminar flame parameters on the normalization of DNS statistics, canonical opposed flames were also simulated. For the present cases, these parameters were found to have negligible effect on the normalized statistics and observations, and hence unperturbed laminar flames parameters are used for normalization. The details of the strained laminar flames can be found in the supplementary section S.2. It is seen that most of the pdfs appear as nearly Gaussian with positive skewness, consistent with the negative skewness of the logarithm of SDR for passive scalar pdfs. The $c_0 = 0.01$ pdf is the broadest with relatively small skewness. Interestingly, for both the *Da*- and *Da*+ cases (in Figs. 3(a) and 3(b), respectively) the position of the pdfs shifts towards the left with increasing c_0, showing that the mean of the flame thickness becomes progressively smaller than its corresponding laminar value, as the conditioning temperature moves towards the burnt gases. In all cases, except $c_0 = 0.01$, the ratio $\langle\delta_L\rangle/\delta_{L,Lam}$ is smaller than unity. Angled brackets are used to denote un-weighted arithmetic average. Therefore, these observations suggest that the flame is progressively thinned, in the mean. The statistics of δ_L are presented in tables A and C for *Da*- and *Da*+, respectively, in the supplementary material section S.4. This observation of progressive thinning is different from the results in [17], which reported progressive flame thickening for stoichiometric H_2-air flames in a statistically planar configuration. The difference in the observations stems, in part, from the strong shear that the flame is subjected to in the present study, which has an overall thinning effect. The geometric configuration used for the simulation in [17] is also different from the one used in the present study. Additionally, for a lean H_2-air flame, heat release rate occurs near free-stream temperatures, and consequently the width of the preheat zone is reduced relative to that in hydrocarbon flames since the activation energies for H_2-air flames are lower than those of hydrocarbon-air flames. This is captured in the present study, as the chemistry was modeled with a detailed mechanism [18]. A single step reaction mechanism with large activation energy, as used by [17], would result in a broad preheat zone with the heat release occurring at near-adiabatic flame temperatures, *i.e.* near fully burnt conditions. As will be shown later, these chemical kinetics considerations are manifested through Lewis number effects. These differences, *i.e.* strong mean shear, geometric configuration, and detailed chemical

mechanism are primarily responsible for the differences in the statistical trends observed in the present study and those in [17].

As defined earlier, the "geometric" flame thickness is also analyzed. Three cases are shown in Figs. 3(a) and 3(b): the black circles correspond to $(c_0, c_1) \equiv (0.10,0.30)$ and the dark and light gray symbols correspond to $(c_0, c_1) \equiv (0.30,0.46)$ and $(c_0, c_1) \equiv (0.30,0.90)$, respectively. For c_0 and c_1 values that are close to one another, the $\delta_{L,geom}$ and δ_L pdfs show reasonable agreement. When the difference is large the respective pdfs are still qualitatively similar, but with a greater degree of quantitative difference. This is not unreasonable as two iso-scalar surfaces that are considerably separated physically may have a greater chance of a non-monotonic temperature profile between them. The pdfs for $(c_0, c_1) \equiv (0.10,0.30)$ and $(c_0, c_1) \equiv (0.30,0.46)$ are nearly identical, showing predominant thinning behavior irrespective of the location of c_1 in the pre-heat zone or the post pre-heat zone. Thus, the observation of flame thinning, is also confirmed with the geometric flame thickness definition. Since, the observations using eq. (2) and eq. (4) do not differ substantially, the discussion henceforth considers the definition of flame thickness based on the local scalar gradient, eq. (2).

Additionally, it is observed that the progressive flame thinning is also independent of the choice of scalar, i.e., T or Y_{O_2}. The pdfs of flame thickness based on $c_{Y_{O_2}}$ can be found in the supplementary material (section S.1).

4.2 Pdfs of CSDR

The pdfs of the logarithm of CSDR are shown in Figs. 4(a) and 4(b) for *Da*- and *Da*+, respectively. These pdfs are a mirror reflection of Figs. 3(a) and 3(b), since $\delta_L \sim \chi_{T_0}^{-1/2}$. The negative skewness is clearly apparent. The pdfs show that the mean of the normalized CSDR increases with increasing values of c. Since the CSDR is normalized by the corresponding CSDR of a planar laminar premixed flame at $c = c_0$, such a behavior can only be an effect of shear-turbulence-flame interaction.

The turbulence-flame interaction can be quantified by examining the transport equation for the SDR [29], where SDR is defined as $N_c = \kappa(\boldsymbol{\nabla} c . \boldsymbol{\nabla} c)$, *i.e.* including the corresponding diffusivity κ,

$$\rho\frac{DN_c}{Dt}=\frac{\partial}{\partial x_j}\left(\rho D\frac{\partial N_c}{\partial x_j}\right)-2\rho\kappa\kappa\left[\frac{\partial}{\partial x_j}\left(\frac{\partial c}{\partial x_j}\right)\right]^2-2\rho\kappa\frac{\partial c}{\partial x_i}S_{ij}\frac{\partial c}{\partial x_j}+2\rho N_c\left(\frac{\partial u_l}{\partial x_l}\right)+2\kappa\frac{\partial c}{\partial x_i}\frac{\partial\dot{\omega}}{\partial x_i} \quad (5)$$

It is well known that the third term on the RHS of eq. (5) is the turbulence scalar interaction term, and whether it represents a source or sink depends on the preferential alignment of the scalar gradients with the directions of eigenvectors of the S_{ij} and the corresponding eigenvalues. Physically, the effect of turbulence is to stretch and wrinkle the isothermal or other iso-scalar surfaces within the flame structure at a multitude of length scales. This straining action is most effective when the eigenvectors of S_{ij} align with the normal and tangential directions of an iso-scalar surface. This is guaranteed (on average) for the passive iso-scalar surfaces [30] but not for a reactive scalar [11]. In three-dimensional non-reacting flows at least one eigenvalue must be compressive to satisfy the incompressibility constraint, *i.e.* the sum of the three eigenvalues (principal strain rates) must be zero. However, with strong heat release in flames all three eigenvalues may be positive showing stretching to dominate along all the eigenvectors. Therefore, unlike non-reacting flows where alignment of the most compressive principal strain rate along the local normal guarantees scalar gradient production, alignment of a eigenvectors of S_{ij} along the local normal, in a flame, may cause scalar gradient production (flame thinning) or dissipation (flame thickening) depending on the magnitude of the heat release rate which alters the arithmetic sign of the eigenvalues. In addition, a detailed reaction mechanism has a significant effect on the heat release rate profile for H_2-air flames, as already discussed. Furthermore, an important point to note, as mentioned in the Introduction, is that in premixed flames not only are fluid strain rates important, but the strain rate due to self-propagation is also important. As such the latter is a measure of the degree to which a flame responds to turbulence. In section 4.4, we have explored the pdfs of the alignment of the eigenvectors of S_{ij} with respect to the normal to the iso-scalar surface to highlight the fact that this analysis alone does not completely explain the flame thinning or thickening mechanism. Here, we proceed to explain the pdfs of flame thickness and CSDR using the evolution equation for the scalar gradient [31, 32] as mentioned below.

$$\frac{\widetilde{D}|\boldsymbol{\nabla}T|}{\widetilde{D}t}=-\left(a_N+\frac{\partial S_d}{\partial n}\right)|\boldsymbol{\nabla}T| \quad (6)$$

$$a_N=\boldsymbol{nn}:\boldsymbol{\nabla u} \quad (7a)$$

$$\frac{\partial S_d}{\partial n} = \boldsymbol{n}.\boldsymbol{\nabla} S_d \tag{7b}$$

$$\boldsymbol{n} = -\frac{\boldsymbol{\nabla} T}{|\boldsymbol{\nabla} T|} \tag{7c}$$

Here, $\widetilde{D}|\boldsymbol{\nabla} T|/\widetilde{D}t$ represents the total derivative of magnitude of the scalar gradient while following the iso-scalar surface (since we deal with isothermal surfaces or constant-property surfaces based on mass fractions of O_2 which have a non-zero flame displacement speed, therefore this derivative is different from the usual material derivative following fluid elements), a_N is the normal strain rate due to fluid motion, $\partial S_d/dn$ is the normal strain rate due to self-propagation, and $\boldsymbol{n}$ is the local normal, where the normal is defined to point towards the unburnt reactants. A relationship has already been established between the magnitude of the scalar gradient and the flame thickness via eq. (2), and between flame thickness and CSDR. Hence, eq. (6) provides a convenient way to interpret the flame thickness and CSDR statistics. We refer to this route as the kinematic route. Positive a_N will separate iso-scalar surfaces and reduce the CSDR; negative values of $\partial S_d/dn$ will bring surfaces closer [31] and increase the CSDR.

The mean of the a_N and $\partial S_d/dn$, for both DNS data sets, are plotted in Fig. 5. The means are normalized by the absolute value of the normal strain rates computed for an unstrained planar laminar flame. As discussed earlier, strong heat release can alter the fluid strain rates. In this study, positive values of mean of a_N are reported for all values of c and *Da*. Thus, the effect of a_N, on average, is to separate the iso-scalar surfaces and reduce the CSDR. However, it can be clearly observed from the plot that the effect of $\partial S_d/dn$ dominates over a_N in magnitude and it is negative. Since S_d, generally, increases from the unburnt to burnt side while the flame normal points towards the unburnt side, $\partial S_d/dn$ will usually be negative. The qualitative behavior of this term is similar for all values of c and for both *Da* cases. Since $\partial S_d/dn$ dominates, it brings two iso-scalar surfaces closer and causes the CSDR to increase (see Figs. 4(a) and 4(b)), and the flame thickness to decrease (see Figs. 3(a) and 3(b)). These observations are consistent with the discussions in [31]. The reason for dominance of $\partial S_d/dn$ is explained below with the help of the chemical kinetics and transport route.

The premixed turbulent flames under consideration have $Le < 1$, and therefore it is possible that the flames exhibit non-unity Lewis number stretch effects. The flames reside in the

shear layer, and, therefore, can be expected to be positively stretched in the mean. In the next sub-section it will be shown that, despite fluctuations in the strain-rates due to turbulence, the mean strain rate on the flame surface is persistent and its effect progressively increases while traversing across the flame towards the products. For a positively stretched flame with $Le < 1$, the burnt gas temperature tends to be super-adiabatic. Furthermore, from classical premixed flame analysis it is known that any $O(\varepsilon)$ change in flame temperature can cause an $O(1)$ change in flame speed, where ε is a small number much less than unity [33]. Thus positive stretch rate causes S_d to increase rapidly along the normal direction and hence $\partial S_d/dn$. This also highlights the coupling between the kinematic route, and the transport and the chemical kinetics route to explain the counter-intuitive thinning of premixed H_2-air turbulent flames.

Chen et al. [34] showed that for lean methane-air turbulent Bunsen flames, the CSDR is always greater than the planar laminar CSDR for $c_0 \leq 0.6$, and is less than that for $c_0 > 0.6$ depending on the axial location of measurement. However, this is not found to be the case for the present study. Figures 6(a) and 6(b) clearly show that for both turbulent cases, *Da*- and *Da*+ respectively, the $\langle|\boldsymbol{\nabla} c|\rangle$ and hence the CSDR at all times of interest $\left(12 \leq t/t_j \leq 20\right)$ are greater than the corresponding laminar $|\boldsymbol{\nabla} c|$ over almost the entire range of the progress variable, except for $c < 0.1$. In addition to providing further validation of the observations in Figs. 3-4, this shows that the flame thinning/increasing CSDR occurs over almost the entire duration of the shear turbulence-flame interaction.

4.3 The effect of mean shear

In contrast to many prior DNS studies, mean shear exists in this configuration causing strong turbulent mixing within the flame structure. As discussed in the previous sub-section, the persistent mean shear can couple with the sub-unity *Le* and result in large negative values of $\partial S_d/dn$. Therefore, a detailed explanation is needed for the effect of mean shear in governing the flame thickness and CSDR statistics.

In this section we investigate the persistence of mean shear and its effect. This could be quantitatively addressed by exploring the ratio, *F,* defined as:

$$F = \frac{\left[\left(\delta_{ij} - \langle n_i n_j \rangle\right)\langle S_{ij}\rangle\right]_{c=c_0}}{\langle\left[\left(\delta_{ij} - n_i n_j\right)S_{ij}\right]_{c=c_0}\rangle_s} \tag{8}$$

where the subscript s denotes surface averaging and δ_{ij} is the Kronecker delta function. The numerator provides the strain rate imposed by the mean velocity gradients on the surface-averaged flame orientation. The denominator denotes mean tangential strain rate on the iso-scalar surface $c = c_0$ and captures the strain rate that the surface experiences due to both mean shear as well as turbulent strain. Hence, the denominator captures the total tangential strain rate due to turbulence, and the smaller the ratio, the more dominant turbulent straining. In the two extreme limits, for a statistically planar flame in homogeneous isotropic turbulence, the factor $F = 0$, whereas for a planar laminar strained premixed flame between two opposed jets, $F = 1$. Hence *F* quantitatively determines the degree to which strain rate due to mean shear or turbulent strain is dominant. However, it needs to be recognized that the entire denominator may not be persistent in time, and so it is not be readily obvious whether mean shear or turbulent strain will couple with *Le* effects. This topic is discussed in detail in describing the trends observed in Figs. 7(a), 7(b), 9(a), and 9(c). The variations of the ratio *F* over different progress variable (temperature based) iso-scalar surfaces for both *Da*- and *Da*+ cases are shown in Fig. 7(a). This figure suggests that the flame encounters more intense turbulence straining with decreasing *Da*. However, for both cases *F* increases with c_0 suggesting an increase in relative importance of mean shear traversing across the flame. We also observed progressive flame thinning with increasing c_0 values, as discussed earlier. Figure 7(b) shows the numerator and denominator of *F*.

Clearly, the total mean tangential strain rate, *i.e.* denominator of *F* for *Da*- , is much larger than that for *Da*+ although it rapidly decreases with c_0 as the local turbulence Reynolds number decreases towards the products. The variation of the local turbulent Reynolds number is plotted in Figure 8, and it decreases faster for the *Da*- case. The numerator of *F* remains nearly constant for most c_0 values and its persistence is due to its origin from the mean velocity gradients and flame surface orientations. The denominator reflects contributions from turbulent straining and hence should be more intermittent in nature. Therefore, flame thinning with increasing progress variable is attributed to the increase in the relative importance of the persistent mean strain rate, as shown in Fig. 7(a) and (b).

Figure 9(a) shows that mean heat release rate (hrr) for *Da*+ is slightly greater than mean hrr for *Da*- which is again greater than that for an unstrained laminar flame, at nearly all c_0 values. Figure 7(a) already showed that *Da*+ case is characterized by larger *F* values in comparison to *Da*-

case. Larger values of F imply relatively greater influence of mean strain rates. Persistent mean strain rates thus could couple with sub-unity *Le* to increase heat release rate across the flame.

A question could still arise on whether this increased heat release rate is caused by the mean strain due to velocity gradients in the shear layer or by the overall turbulent strain. This can be explained by considering the quantity: $\langle\left[\left(\delta_{ij}-n_i n_j\right)S_{ij}\right]_{c=c_0}\rangle \times \tau_{Kol}$. It was observed in [35] that the Markstein number response to fluctuating tangential strain rate dropped sharply when the time scale of strain rate fluctuations was of the same order as that of the mean strain rate for a counter-flow laminar premixed flame. In a strongly turbulent flow, according to [36], the time scale of tangential strain rate fluctuations on a propagating surface could be considered proportional to the Kolmogorov time scale: $\tau_{Kol}=\left(\tilde{\nu}/\tilde{\varepsilon}\right)^{1/2}$. Here, $\tilde{\varepsilon}$ is the Favre-averaged mean dissipation rate. τ_{Kol} is evaluated on each surface corresponding to the progress variable values to account for the effect of combustion on the Kolmogorov microscales. Figure 9(b) shows the increasing τ_{Kol} with respect to the progress variable. Therefore the factor $\langle\left[\left(\delta_{ij}-n_i n_j\right)S_{ij}\right]_{c=c_0}\rangle \times \tau_{Kol}$ can be examined to determine whether strain rate fluctuations are persistent long enough to affect the flame thickness through augmented transport and heat release, *i.e.* through sub-unity *Le* effects. As seen from Fig. 9(c) for both *Da*- and *Da*+ cases, $\langle\left[\left(\delta_{ij}-n_i n_j\right)S_{ij}\right]_{c=c_0}\rangle \times \tau_{Kol} < 1$ within the entire flame region, suggesting that strain rate fluctuations occur over time scales much faster than that required for transport to be affected.

Therefore, it follows from the discussion concerning Fig. 7-9 that the effect of mean shear is persistent, and is dominant over the fluctuating strain rates due to turbulence. It further couples with sub-unity *Le* to cause an increase in the heat release rate and the effect of mean shear increases across the flame. Consequently, the $\partial S_d/dn$ dominate over the a_N over the entire flame region bringing the iso-scalar surfaces closer together resulting in reduced flame thickness and increased CSDR. These observations are consistent with those in [31] performed in the corrugated flamelet regime where the $\partial S_d/dn$ was found to be negative and was much greater than the a_N enhancing molecular diffusive transport and chemical conversion. In [32], analysis of the flame thickness using the transport equation for the magnitude of the scalar gradient, eq.(6), similar to this paper, was reported for a reduced methane-air mechanism in the thin reaction zones regime. However, it was observed that the mean thickness of the turbulent flame is greater than that of the corresponding laminar flame. The differences in observations may be due to the different reaction

mechanism of CH_4-air. For H_2-air a significant amount of heat release occurs near the free-stream conditions, whereas for CH_4-air in [32], the heat release layer was not significantly perturbed. Additionally, the flame in [32] was simulated in a different geometric configuration.

4.4 Pdfs of eigenvector alignment

We now explore the pdfs of the alignment of eigenvectors of the fluid deformation rate tensor S_{ij} with the scalar gradient or local normal. We also qualitatively discuss the effects of progressively dominating mean shear and diminishing fluctuating fluid strain rates on the alignment statistics. It has already been discussed that strong heat release rate can alter the eigenvalues of S_{ij} and that the smallest eigenvalue of S_{ij} need not always be negative. In fact, in the present study the smallest eigenvalue is nearly positive in the mean (see Fig. 5).

The alignments of the eigenvector corresponding to the largest and the smallest principal strain rate with the normal to the iso-scalar surface are shown in Figs. 10(a) and 10(b), respectively, for the *Da*- case. Clearly for all c_0 values (for $c_0 = 0.01$ and 0.1 to 0.9 in increments of 0.1) the iso-scalar surface normal is strongly aligned with the smallest strain rate. Though this alignment behavior seems similar to the alignment of the most compressive strain rate with the normal to the iso-scalar surface for a passive scalar in non-reacting turbulence, in the present study with reactive scalars this corresponds to the eigenvalue which, on average, is the smallest positive quantity among the three principal strain rates at each location. Here θ_γ is the angle between the isothermal surface normal and the eigenvector corresponding to smallest principal strain rate. Similar trends are observed for the *Da*+ case as well and the corresponding plots can be found in the supplementary section S.3.

The implication is that for both cases with increasing c_0 the smallest principal strain rate, which is predominantly positive and hence extensive, becomes increasingly efficient at separating two adjacent iso-scalar surfaces. The increasing strength of the preferential alignment between the normal to the iso-scalar surfaces and the smallest strain rate with increasing c_0 can be explained as follows. All of the wrinkled iso-scalar surfaces of c reside in the shear layer of the jet for the time instant of interest, $t/t_j = 15$. Furthermore, low c or T iso-scalar surfaces are highly wrinkled due to the large local turbulence Reynolds number: Re_{T,c_0} of the fresh reactants, due to small values of the kinematic viscosity. However, with increasing temperature viscosity increases leading to decreasing Re_{T,c_0}. This was shown in Fig. 8 for the *Da*- and *Da*+ cases. In addition,

through the previous analysis of the factor F, it was also shown that the effect of the mean shear remains persistent while that of turbulent fluctuating strain-rate diminishes while traversing towards the burnt side of the flame. Hence, large c or T iso-scalar surfaces are less wrinkled and are flatter (than their low c or T counterparts), thereby allowing their surface normal to be better aligned with the direction of the smallest principal strain rate.

As such, the increasing strength of preferential alignment with the total strain rate is expected to be a general attribute of premixed flames embedded in a shear layer. At the same time we recognize that the c_0 value from which the mean CSDR becomes greater than (or less than) the corresponding planar laminar value is sensitive to the distribution of heat release rate within the flame structure. However, as discussed previously, although a_N become increasingly efficient in separating iso-scalar surfaces, its effect is overshadowed by $\partial S_d/dn$ which is a kinematic manifestation of the coupling between the mean shear and the sub-unity Le. Therefore, it can also be said that the alignment statistics of the eigenvectors of the S_{ij} with the local normal alone do not completely quantify the flame thickening and thinning behavior since the effect of strains due to varying flame displacement speed is not accounted in S_{ij}, by definition.

4.5 Intermittency of CSDR

At high Ka in the thin reaction zones regime there is considerable scatter in the CSDR due to highly transient flame-flame interactions. Understanding the degree of scatter and the nature of the intermittency associated with CSDR is important for the development of mixing models used in engineering simulations, *e.g.* Large-Eddy Simulation (LES) with sub-grid filtered density function approach. A recent study by [37] has identified that there is significant degree of scatter in the present DNS data, by over an order of magnitude, due in part to highly transient flame processes including flame self-interaction. Hence, it is of both fundamental and practical interest to characterize the intermittency of the CSDR across the flame.

In Figs. 11(a) and 11(b), the CSDR (based on temperature) data presented in Figs. 4(a) and 4(b) are re-plotted; the interest here is to understand the tails of the pdfs, *i.e.* the intermittent behavior of the CSDR within the flame structure. Hence in Figs. 11(a) and 11(b), the CSDR is normalized with the corresponding ensemble mean of the conditional variable. For a passive scalar dissipation rate, there is some debate in the literature as to whether the pdf tail is lognormal or a stretched exponential, *i.e.* an exponential function with an exponent less then unity: $exp(-x^{\beta})$,

with $\beta < 1$. Using the Kraichnan model, *i.e.* random laminar flow smoothly varying in space but delta correlated in time to force the exact passive scalar governing equation, Chertkov *et al.* [38] analytically showed that the steady pdf of the passive scalar dissipation rate is well represented by a stretched exponential and suggested that the lognormal unsteady distribution could only be realized without diffusion. In Figs. 11(a) and 11(b), the pdfs of the CSDR conditioned at $c_0 = 0.01$ and 0.1 to 0.9 in increments of 0.1 are plotted for the *Da*- and *Da*+ cases at $t/t_j = 15$, respectively. In Fig. 11(a) (*Da*-) the pdf of the CSDR conditioned at $c_0 = 0.01$ exhibits a stretched exponential behavior as expected for a passive scalar. However with incremental progress across the flame structure, at $c_0 = 0.01$ the stretched exponential tail of the CSDR pdf is cut off dramatically to yield a compressed exponential pdf. An almost perfect exponential pdf is obtained at $c_0 = 0.3$. For a planar laminar premixed flame $c_0 = 0.3$ also coincides with the location of the maximum heat release rate. The dramatic cutoff of the stretched exponential tails, immediately within the flame structure, can be understood by considering the chemical structure of a hydrogen flame, realized with a detailed chemical mechanism. In hydrogen-air laminar premixed flames, the bulk heat release occurs towards the free-stream. For hydrogen systems, the early heat release rate originates predominantly from the three-body recombination reaction: $H + O_2 + M \Leftrightarrow HO_2 + M$ which has zero activation energy. At this location the H atom produced downstream back diffuses to react with O_2 in the inflowing H_2-air mixture [33]. The heat release rate versus c shown in the inset of Fig. 11(a) sharply rises at small values of c, peaks at $c_0 = 0.3$, and gradually becomes negligible by $c_0 = 0.8$. This behavior is perfectly reflected in the tails of the CSDR pdfs in Fig. 11 as well. After $c_0 = 0.3$ the tails of the CSDR pdfs slowly relax and by $c_0 = 0.9$ it becomes quantitatively identical to the tail at $c_0 = 0.01$, returning to the passive scalar stretched exponential behavior. In between $0.5 \leq c_0 \leq 0.8$ the tails of the pdfs are predominantly stretched exponentials except for $pdf < 10^{-4}$ where the stretched tails are rounded off. In Fig. 11(b) (*Da*+) the normalized CSDR pdf at $c_0 = 0.01$ is a well stretched exponential like a passive scalar only to show compressed exponential behavior at $0.1 \leq c_0 \leq 0.3$, exponential behavior at $c_0 = 0.3$ and returning again to stretched exponential behavior between $0.3 \leq c_0 \leq 0.9$. In Fig. 11(c) and 11(d), the CSDR based on the O_2 mass fraction, normalized by its mean, is plotted for the *Da*- and *Da*+ cases respectively.

In Fig. 12(a) we plot the value of the exponent β, obtained by nonlinear fitting of the CSDR (based on temperature) pdf tails for both *Da*- and *Da*+ with the stretched exponential function:

$$p\left(\chi_{T_0} \gg \langle\chi_{T_0}\rangle\right) = C_1\chi_{T_0}^{-1/2} exp\left(-C_2\chi_{T_0}^{\beta}\right) \quad (9)$$

following [38] and [39]. Here we find that for $0.1 \leq c_0 \leq 0.3$ the CSDR pdfs are compressed exponential or exponential, *i.e.* $\beta \geq 1$, and outside this domain, the CSDR pdfs are stretched exponential, *i.e.* $\beta < 1$. Interestingly the exponent β of the CSDR (based on O_2 mass fraction) pdf tails for both *Da*- and *Da*+ shows a much smoother behavior in Fig. 12(b). This can be attributed to the heat release rate distribution in the $c_{Y_{O_2}}$ space. As shown in the inset of Fig. 11(c), the heat release rate is much more uniform and occurs over a broad range of values of $c_{Y_{O_2}}$ in comparison to its peak and ramp shaped distribution in the c (based on temperature) space shown in the inset of Fig. 11(a). This once again highlights the paramount role of heat release distribution in controlling CSDR intermittency within the flame structure. One obvious implication of the stretched exponential function for CSDR is on modelling closures. The relationship governing SDR, CSDR and the pdf of progress variable is well known, and most modelling methodologies require an independent closure for these quantities. For instance, the well-known conditional moment closure (CMC) approach [41] requires a closure to be provided for CSDR and can directly benefit from Eq. (9).

If the inner structure, that is, the reaction zone or heat release rate zone of the flame is perfectly intact as in a planar laminar flame, the CSDR pdfs in the heat release zones should be well approximated by Dirac delta functions. Any stretch distribution either due to curvature or strain should result in progressive flaring of the tails from this limiting Dirac delta pdf. Therefore, for all values of *Da* or *Ka*, the CSDR pdf in the heat release zone is expected to vary from a Dirac delta function as $Da \to \infty$ for planar laminar flames to a stretched exponential as $Da \to 0$ in a passive scalar in the zero heat release limit for an extinguished condition.

That heat release rate damps intermittency and transforms the stretched exponential pdf to a compressed exponential pdf was also demonstrated by [17]. However, in [17] an implicit large eddy simulation (ILES) technique along with single global step hydrogen-air chemistry was used in a statistically planar premixed flame configuration. A detailed study of intermittency requires fine scale spatial and temporal resolution to resolve the smallest relevant length scale, *i.e.* the Kolmogorov or Batchelor scales. Moreover, a discussion of the statistics of the flame structure requires a detailed description of the relevant chemistry. Both spatial resolution and detailed chemistry are accounted for in the present DNS study. As discussed earlier, a global one-step

chemistry cannot correctly predict the flame structure and for H_2-air flames, it incorrectly predicts the occurrence of heat release rate at near adiabatic flame temperature. As a result, the intermittency (tails of the stretched exponential pdfs) progressively decreases from fresh reactants to burnt products in [17]. This is in direct contrast to the present result and a consequence of the detailed H_2-air combustion chemistry where intermittency is most damped near free stream temperatures due to the occurrence of large heat release at the front of the flame.

5. Conclusion

In the present study the mean and intermittency of the flame thickness and the CSDR of a lean premixed hydrogen-air flame interacting with intense shear driven turbulence in the thin reaction zones regime is studied at two different *Da*. From statistical analysis two important findings emerge:

i) The mean of the flame thickness, which scales as the square root of the inverse of the CSDR, conditioned on different progress variable iso-scalar surfaces is predominantly smaller than the corresponding planar laminar flame thickness. The normalized values become smaller with increasing conditioning value of the progress variable. This observation persists even when a purely geometric definition of the flame thickness is used, and is also insensitive to the definition of progress variable. It is observed that the persistent mean strain rates originating from the mean velocity gradients: $\langle S_{ij} \rangle$ and orientation factor: $\langle n_i n_j \rangle$ due to flame propagation within a jet shear layer is a major reason for the counter-intuitive thinning. The persistent mean strain rates couple with sub-unity *Le* resulting in increased heat release over the flame region. This causes the normal strain rates due to self-propagation to dominate over the normal strain rates due to fluid flow, which overall, causes the iso-scalar surfaces of the flame to come closer together, effectively decreasing the flame thickness and increasing the CSDR. Additionally, it has been noted that the alignment of the eigenvectors of the S_{ij} with the local normal alone, cannot explain the flame thickening or thinning effect and the strain rates due to self-propagation should also be taken into account.

ii) The tails of the pdf of the CSDR are well represented by stretched exponential functions when they are conditioned on iso-scalar surfaces with progress variable near zero values (0.01). At this upstream location the CSDR is a strongly intermittent variable as expected for a passive scalar.

Immediately into the flame structure (for $c = 0.1$ and greater) the pdf tails become compressed exponentials to slowly relax again to the stretched exponential behavior at large progress variable values near unity. Such a non-monotonic behavior of the exponent of the exponential pdf, with crossover from greater than unity (compressed exponential) to less than unity (stretched exponential) occurring at the peak heat release location, is attributed to the unique structure of premixed hydrogen-air flames where heat release is generated at near free stream temperature.

Acknowledgements: The authors would like to thank Dr. H. Yu of the University of Nebraska for generating the images in Figs. 1(a) and (b). This work was supported by the Combustion Energy Frontier Research Center, an Energy Frontier Research Center funded by the U.S. Department of Energy, Office of Basic Energy Sciences under Award Number DE-SC0001198, awarded to the Sandia National Laboratories and Princeton University, and by the U.S. National Science Foundation awarded to Princeton University. J.H. Chen also acknowledges the support of OLCF computational resources via INCITE, and E. Hawkes acknowledges the support of the Australian Research Council and the National Computational Infrastructure, Australia.

References:

[1] E.R. Hawkes, O. Chatakonda, H. Kolla, A.R. Kerstein, J.H. Chen, A petascale direct numerical simulation study of the modelling of flame wrinkling for large-eddy simulations in intense turbulence, Combustion and Flame 159 (2012) 2690-2703.
[2] N. Peters, Laminar diffusion flamelet models in non-premixed turbulent combustion, Progress in energy and combustion science 10 (1984) 319-339.
[3] D.B. Spalding, Mixing and chemical reaction in steady confined turbulent flames, Symposium (International) on Combustion 13 (1971) 649-657.
[4] D.B. Spalding. Development of the eddy-break-up model of turbulent combustion. In: editor^editors. Symposium (International) on Combustion; 1977: Elsevier. p. 1657-1663.

[5] K. Bray, J.B. Moss, A unified statistical model of the premixed turbulent flame, Acta Astronautica 4 (1977) 291-319.
[6] K. Bray. The interaction between turbulence and combustion. In: editor^editors. Symposium (International) on Combustion; 1979: Elsevier. p. 223-233.

[7] D. Veynante, L. Vervisch, Turbulent combustion modeling, Progress in energy and combustion science 28 (2002) 193-266.
[8] H. Kolla, J.W. Rogerson, N. Chakraborty, N. Swaminathan, Scalar Dissipation Rate Modeling and Its Validation, Combust Sci Technol 181 (2009) 518-535.
[9] N. Peters, The turbulent burning velocity for large-scale and small-scale turbulence, Journal of Fluid Mechanics 384 (1999) 107-132.
[10] S. Chaudhuri, V. Akkerman, C.K. Law, Spectral formulation of turbulent flame speed with consideration of hydrodynamic instability, Physical Review E 84 (2011).
[11] N. Swaminathan, R.W. Grout, Interaction of turbulence and scalar fields in premixed flames, Physics of Fluids 18 (2006) 045102.
[12] N. Chakraborty, N. Swaminathan, Influence of the Damköhler number on turbulence-scalar interaction in premixed flames. II. Model development, Physics of Fluids (1994-present) 19 (2007) 045104.
[13] N. Chakraborty, N. Swaminathan, Influence of Damkohler number on turbulence-scalar interaction in premixed flames, Part I: physical insight, Physics of Fluids 19 (2007) 045103-.
[14] K.R. Sreenivasan, Possible effects of small-scale intermittency in turbulent reacting flows, Flow Turbul Combust 72 (2004) 115-131.
[15] A.R. Kerstein, Fractal dimension of propagating interfaces in turbulence, Physical Review A 44 (1991).
[16] C. Meneveau, T. Poinsot, Stretching and quenching of flamelets in premixed turbulent combustion, Combustion and Flame 86 (1991) 311-332.
[17] P.E. Hamlington, A.Y. Poludnenko, E.S. Oran, Intermittency in premixed turbulent reacting flows, Physics of Fluids 24 (2012) 075111.
[18] J. Li, Z. Zhao, A. Kazakov, F.L. Dryer, An updated comprehensive kinetic model of hydrogen combustion, International journal of chemical kinetics 36 (2004) 566-575.
[19] V. Moureau, P. Domingo, L. Vervisch, From Large-Eddy Simulation to Direct Numerical Simulation of a lean premixed swirl flame: Filtered laminar flame-PDF modeling, Combust Flame 158 (2011) 1340-1357.
[20] A. Trouvé, The production of premixed flame surface area in turbulent shear flow, Combustion and flame 99 (1994) 687-696.

[21] T. Poinsot, D. Veynante, S. Candel, Quenching processes and premixed turbulent combustion diagrams, Journal of Fluid Mechanics 228 (1991) 561-606.
[22] J. Driscoll, Turbulent premixed combustion: Flamelet structure and its effect on turbulent burning velocities, Progress in Energy and Combustion Science 34 (2008) 91-134.
[23] L.K. Su, N.T. Clemens, The structure of fine-scale scalar mixing in gas-phase planar turbulent jets, Journal of Fluid Mechanics 488 (2003) 1-29.
[24] P. Vedula, P.K. Yeung, R.O. Fox, Dynamics of scalar dissipation in isotropic turbulence: a numerical and modelling study, Journal of Fluid Mechanics 433 (2001) 29-60.
[25] S.P. Nandula, T.M. Brown, R.W. Pitz, Measurements of Scalar Dissipation in the Reaction Zones of Turbulent Nonpremixed H-2 Air Flames, Combustion and Flame 99 (1994) 775-783.
[26] H. Pitsch, H. Steiner, Scalar mixing and dissipation rate in large-eddy simulations of non-premixed turbulent combustion, Proceedings of the Combustion Institute 28 (2000) 41-49.
[27] E.R. Hawkes, R. Sankaran, J.C. Sutherland, J.H. Chen, Scalar mixing in direct numerical simulations of temporally evolving plane jet flames with skeletal CO/H-2 kinetics, Proceedings of the Combustion Institute 31 (2007) 1633-1640.
[28] R.J. Kee, F.M. Rupley, J.A. Miller, Chemkin-II: A Fortran chemical kinetics package for the analysis of gas-phase chemical kinetics, Sandia National Labs., Livermore, CA (USA), 1989.
[29] N. Swaminathan, K. Bray, Effect of dilatation on scalar dissipation in turbulent premixed flames, Combustion and Flame 143 (2005) 549-565.
[30] W.T. Ashurst, A.R. Kerstein, R.M. Kerr, C.H. Gibson, Alignment of vorticity and scalar gradient with strain rate in simulated Navier–Stokes turbulence, Physics of Fluids 30 (1987) 2343.
[31] C. Dopazo, L. Cifuentes, J. Martin, C. Jimenez, Strain rates normal to approaching iso-scalar surfaces in a turbulent premixed flame, Combustion and flame, (2014).
[32] R. Sankaran, E.R. Hawkes, J.H. Chen, T. Lu, C.K. Law, Structure of a spatially developing turbulent lean methane–air Bunsen flame, Proceedings of the combustion institute 31 (2007) 1291-1298.
[33] C.K. Law, Combustion physics, Cambridge University Press, New York, 2006.
[34] J.H. Chen, A. Choudhary, B. De Supinski, M. DeVries, E. Hawkes, S. Klasky, W. Liao, K. Ma, J. Mellor-Crummey, N. Podhorszki, Terascale direct numerical simulations of turbulent combustion using S3D, Comput. Sci. Discovery 2 (2009) 015001.
[35] S. Nair, T.C. Lieuwen, Near-Blowoff Dynamics of a Bluff-Body Stabilized Flame, Journal of Propulsion and Power 23 (2007) 421-427.
[36] P.K. Yeung, S.S. Girimaji, S.B. Pope, Straining and scalar dissipation on material surfaces in turbulence: Implications for flamelets, Combustion and Flame 79 (1990) 340-365.
[37] M. Kuron, E.R. Hawkes, Z. Ren, J.C. Tang, H. Zhou, J.H. Chen, T. Lu, Performance of transported PDF mixing models in a turbulent premixed flame, Proceedings of the Combustion Institute, (2016).
[38] M. Chertkov, G. Falkovich, I. Kolokolov, Intermittent dissipation of a passive scalar in turbulence, Physical Review Letters 80 (1998) 2121-2124.
[39] J. Schumacher, D. Kushnir, A. Brandt, K. Sreenivasan, H. Zilken, Statistics and Geometry in High-Schmidt Number Scalar Mixing, in: M. Oberlack, G. Khujadze, S. Günther, T. Weller, M. Frewer, J. Peinke, S. Barth (Eds.), Progress in Turbulence II, Springer Berlin Heidelberg2007, pp. 235-239.

[41] A.Y. Klimenko, R.W. Bilger, Conditional moment closure for turbulent combustion, Progress in Energy and Combustion Science 25 (1999) 595-687.

Figures:

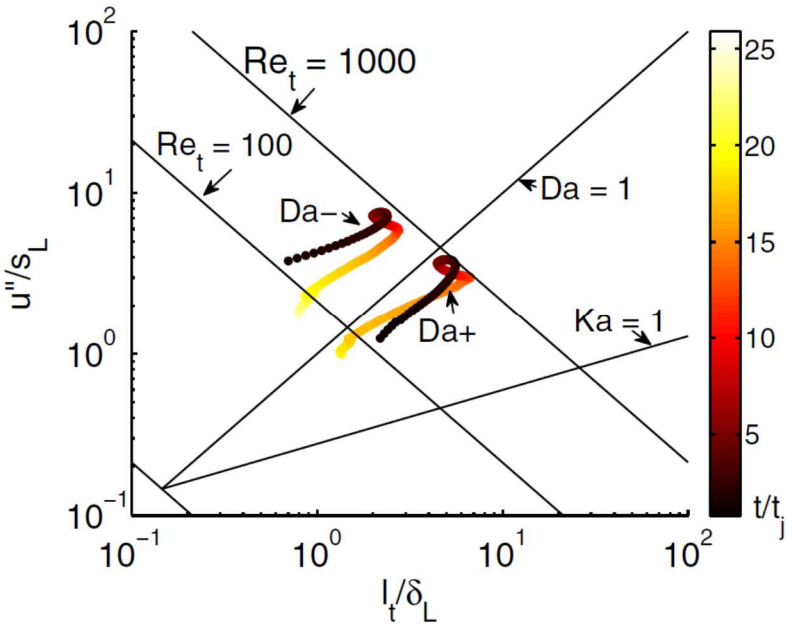

Figure 1: (a) Locus of the maximum turbulence Reynolds number point for the *Da*- and *Da*+ cases. From: [1]

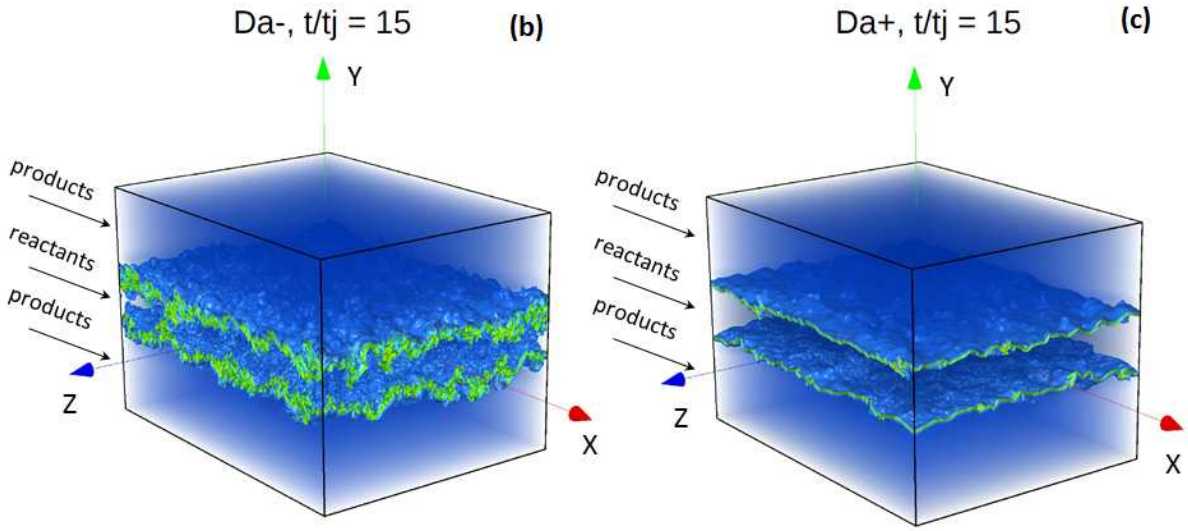

Figure 1: (b) Left: Iso-scalar surfaces of maximum heat release rate for the ***Da-*** case at $t/t_j = 15$.

(c) Right: Iso-scalar surfaces of maximum heat release rate for the ***Da+*** case at $t/t_j = 15$.

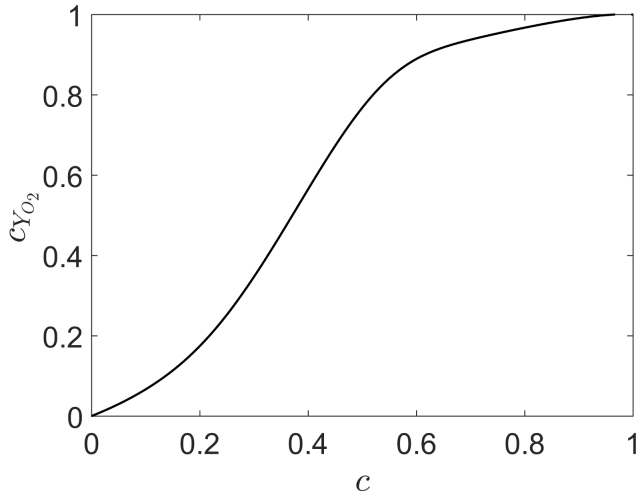

Figure 2: Plot of progress variable based on temperature (x axis) vs. progress variable based on O_2 mass fraction (y axis).

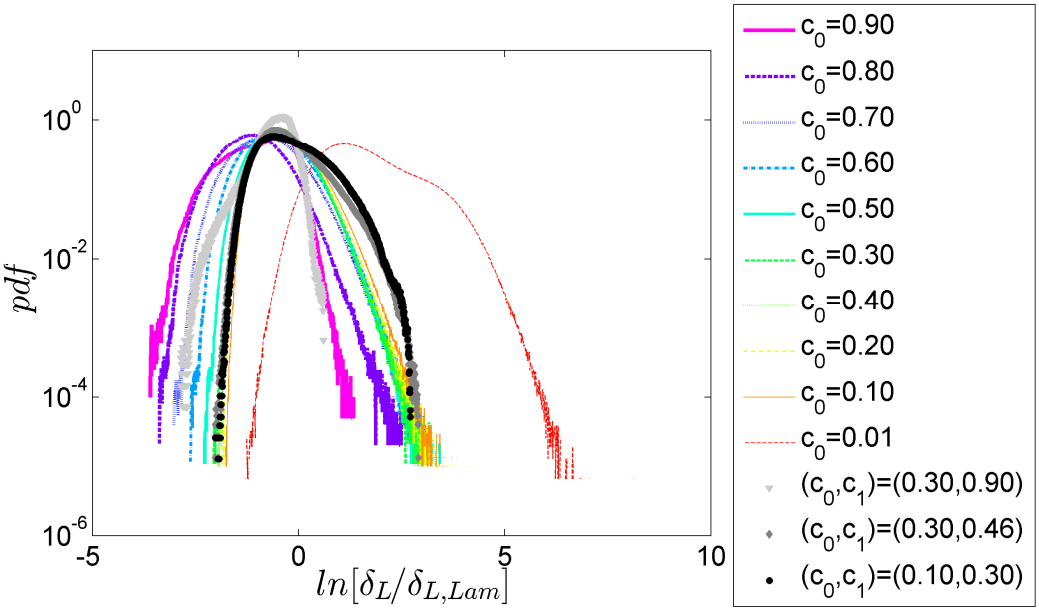

Figure 3: (a) Lines: Probability density function (pdf) of logarithm of δ_L (eq. 2) for the ***Da-*** case normalized by the corresponding unstrained planar laminar flame thickness. Color scale for the lines shown in right. Symbols: Pdf of geometric flame thickness (eq. 3). The black circles correspond to the $(c_0, c_1) \equiv (0.10,0.30)$ and the gray circles correspond to $(c_0, c_1) \equiv (0.30,0.46)$ and $(c_0, c_1) \equiv (0.30,0.90)$

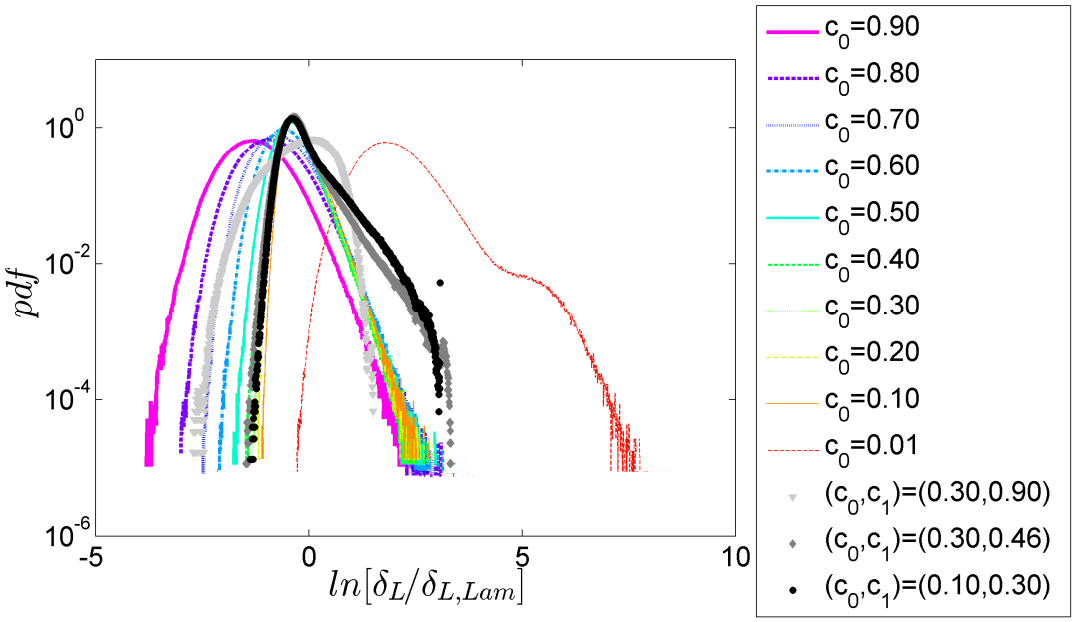

Figure 3: (b) Lines: Probability density function (pdf) of logarithm of δ_L (eq. 2) for the ***Da+*** case normalized by the corresponding planar laminar flame thickness. Color scale for the lines shown in right. Symbols: Pdf of geometric flame thickness (eq. 3). The black circles correspond to the $(c_0, c_1) \equiv (0.10,0.30)$ and the gray circles correspond to $(c_0, c_1) \equiv (0.30,0.46)$ and $(c_0, c_1) \equiv (0.30,0.90)$

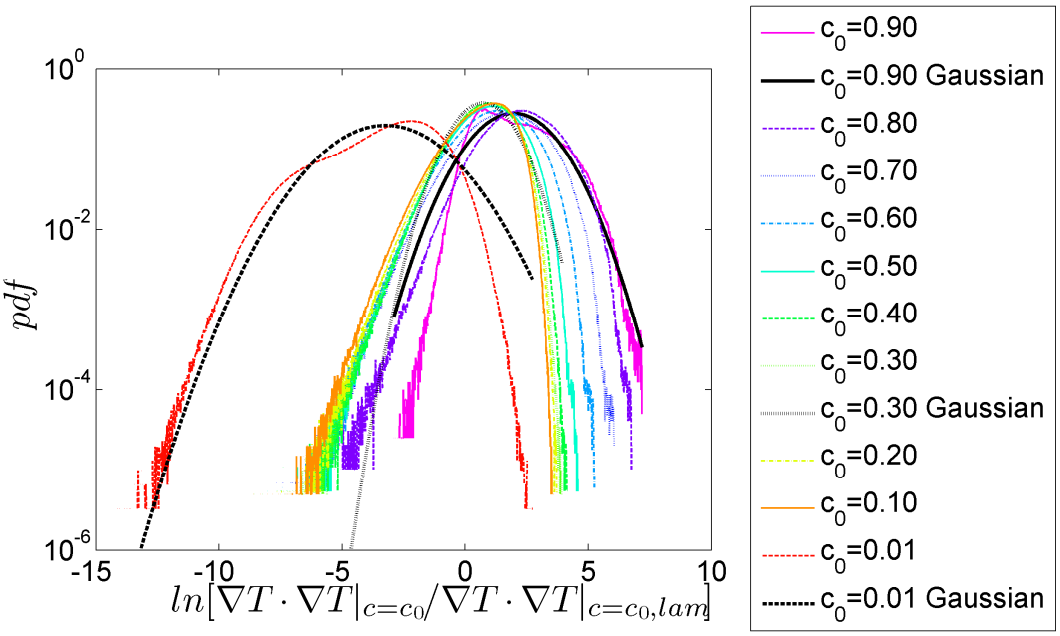

Figure 4: (a) Probability density function (pdf) of logarithm of CSDR (eq. 3) for the ***Da-*** case normalized by the corresponding planar laminar flame thickness. The black lines show the Gaussian distributions with mean and standard deviations equal to that of the logarithm of normalized CSDR at the corresponding iso-scalar surface.

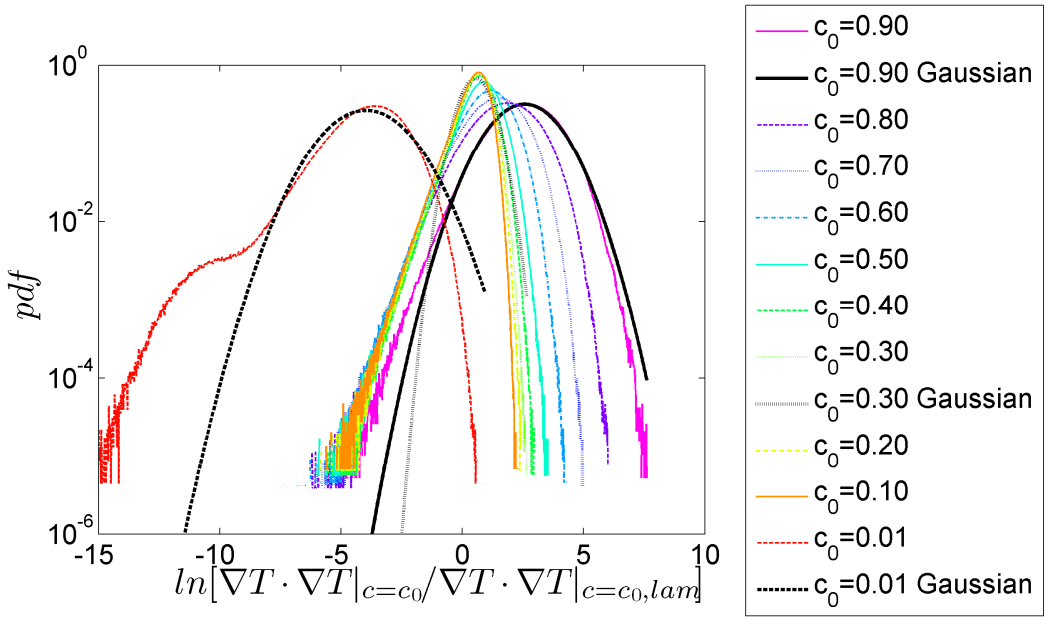

Figure 4: (b) Probability density function (pdf) of logarithm of CSDR (eq. 3) for the ***Da+*** case normalized by the corresponding planar laminar flame thickness. The black lines show the Gaussian distributions with mean and standard deviations equal to that of the logarithm of normalized CSDR at the corresponding iso-scalar surface.

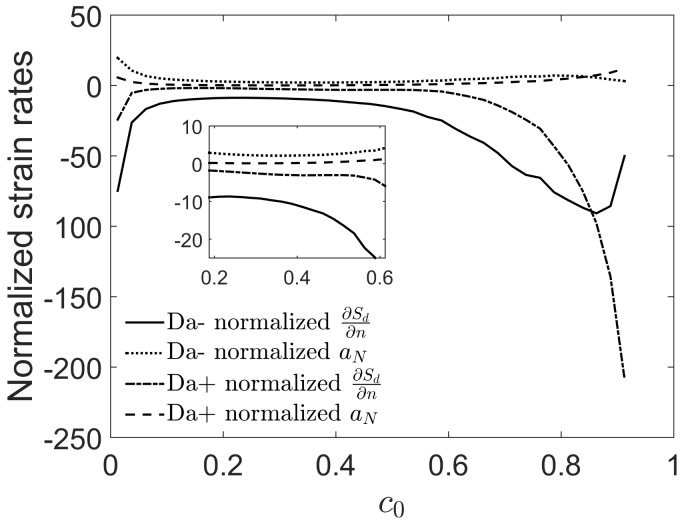

Figure 5: Comparison of normalized statistics of fluid normal strain, a_N, and normal strain due to self-propagation, $\partial S_d / dn$, for both ***Da-*** and ***Da+*** case. The inset shows the plots with c_0 ranging from 0.2 to 0.6.

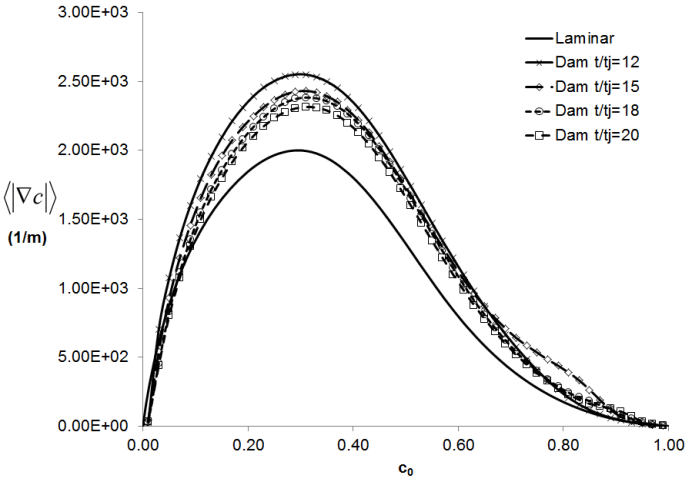

Figure 6: (a) Plot of the conditional mean of absolute gradient of progress variable vs. progress variable based on temperature for the ***Da-*** case at different times.

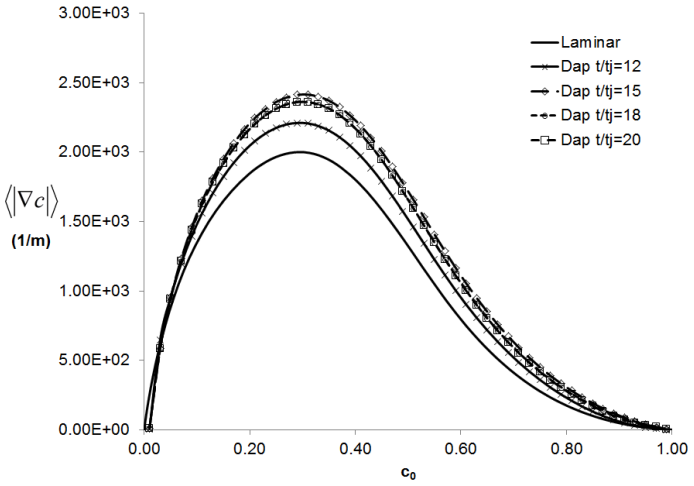

Figure 6: (b) Plot of the conditional mean of the absolute gradient of progress variable vs. progress variable based on temperature for the ***Da+*** case at different times.

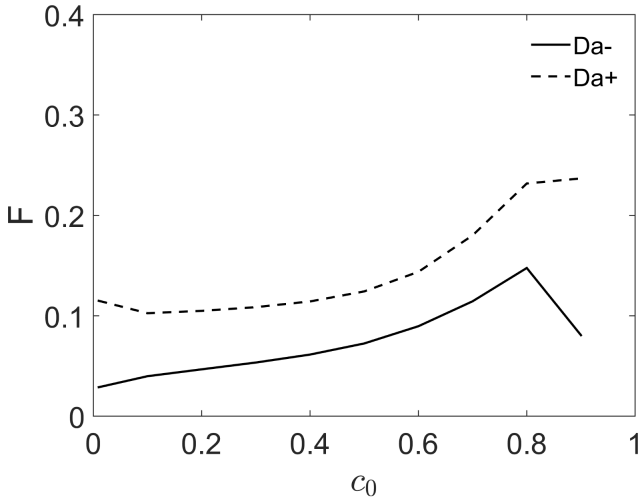

Figure 7: (a) Variation of the factor *F* as a function of progress variable for *Da-* and *Da+* cases.

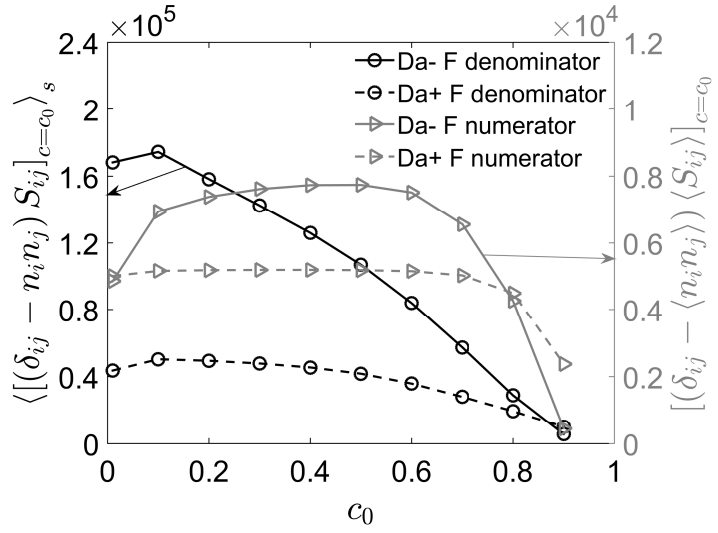

Figure 7: (b) Variation of the numerator and denominator of the factor *F* as a function of the progress variable for *Da-* and *Da+* cases.

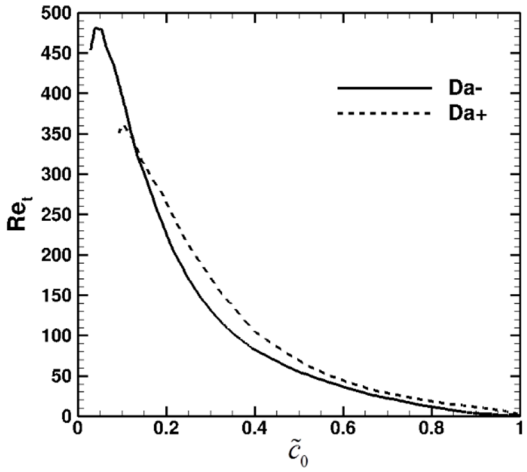

Figure 8: Variation of turbulence Reynolds number based on integral length scale $l_T = u''/\tilde{\varepsilon}$ (where u'' is the root mean square of velocity fluctuations and $\tilde{\varepsilon}$ the mean dissipation rate) inside the flame structure for ***Da-*** and ***Da+*** cases. $\tilde{c}_0$ in the abscissa is the Favre averaged progress variable based on temperature.

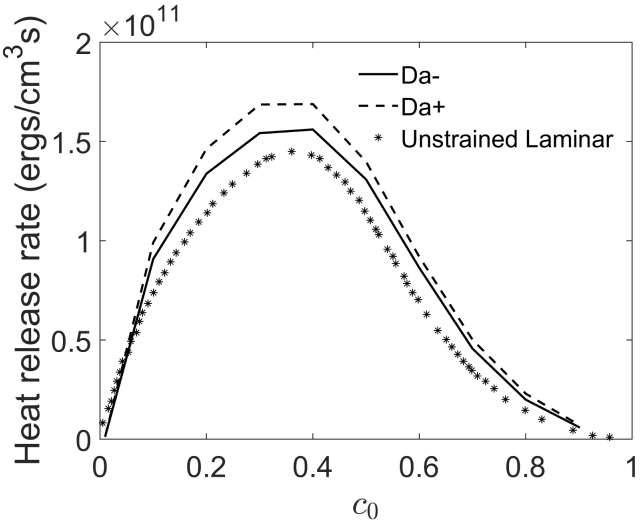

Figure 9: (a) Distribution of heat release rate within the flame thickness for *Da-*, *Da+* and planar unstrained laminar flame.

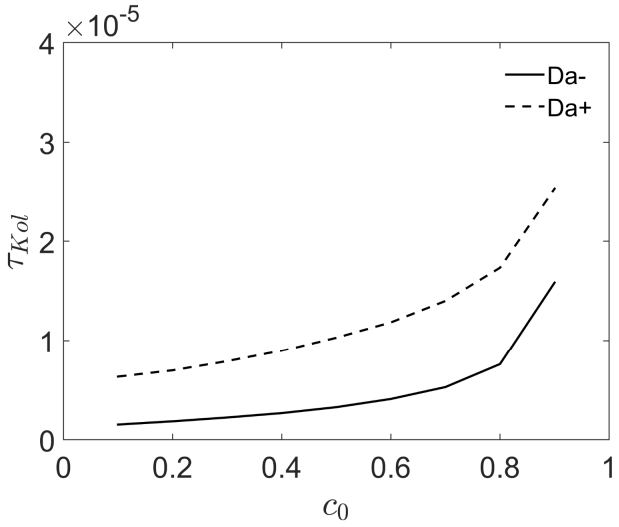

Figure 9: (b) Variation of Kolmogorov timescales with respect to progress variable in Da- and Da+ turbulent flames

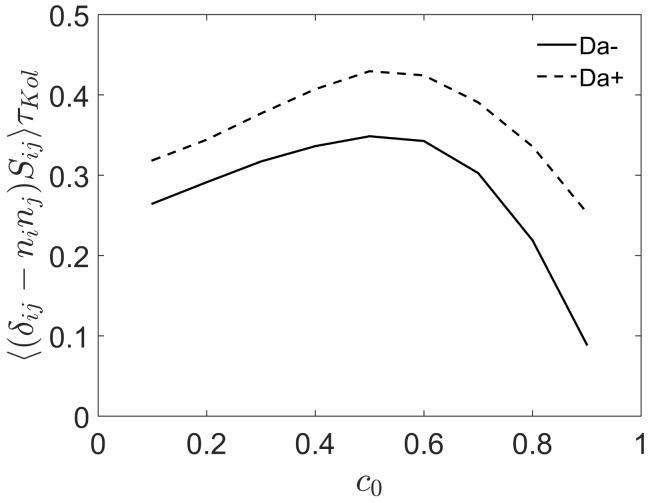

Figure 9: (c) Product of mean tangential strain rate and local Kolmogorov time scale for *Da*-, *Da*+ cases.

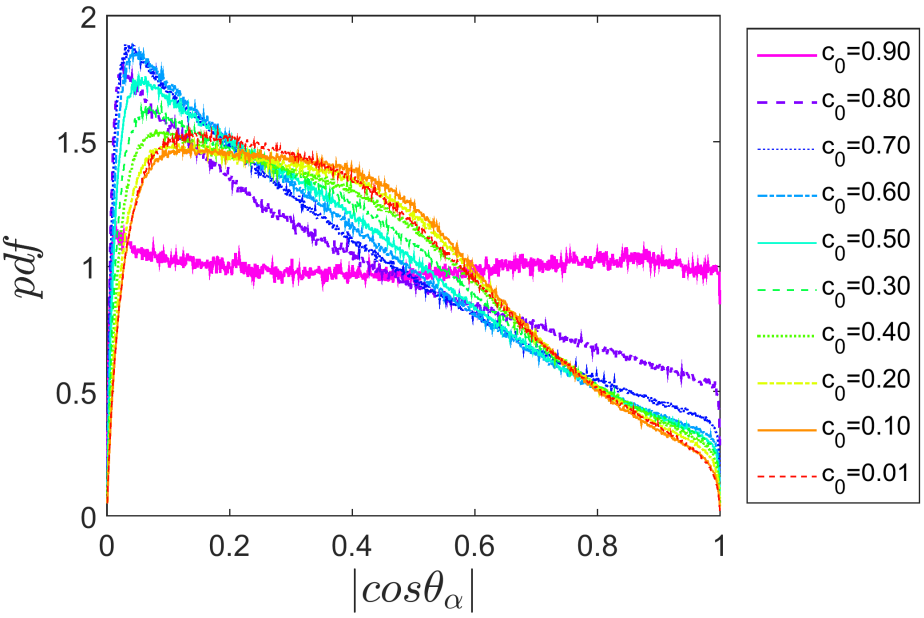

Figure 10: (a) Pdf of alignment between the largest principal strain rate (total) and the corresponding normal to the iso-scalar surface for ***Da-*** case.

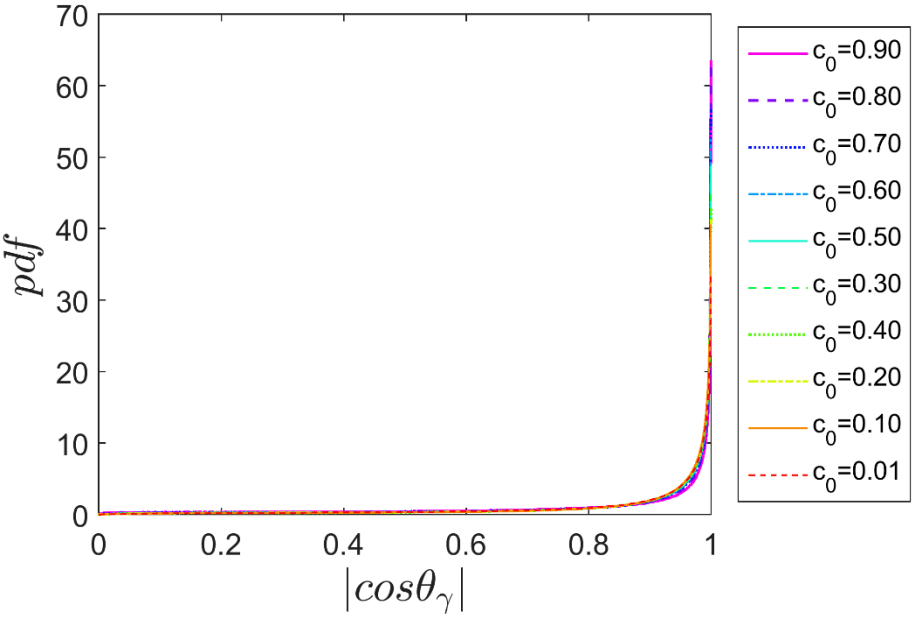

Figure 10: (b) Pdf of alignment between the smallest principal strain rate (total) and the corresponding normal to the iso-scalar surface for the ***Da-*** case.

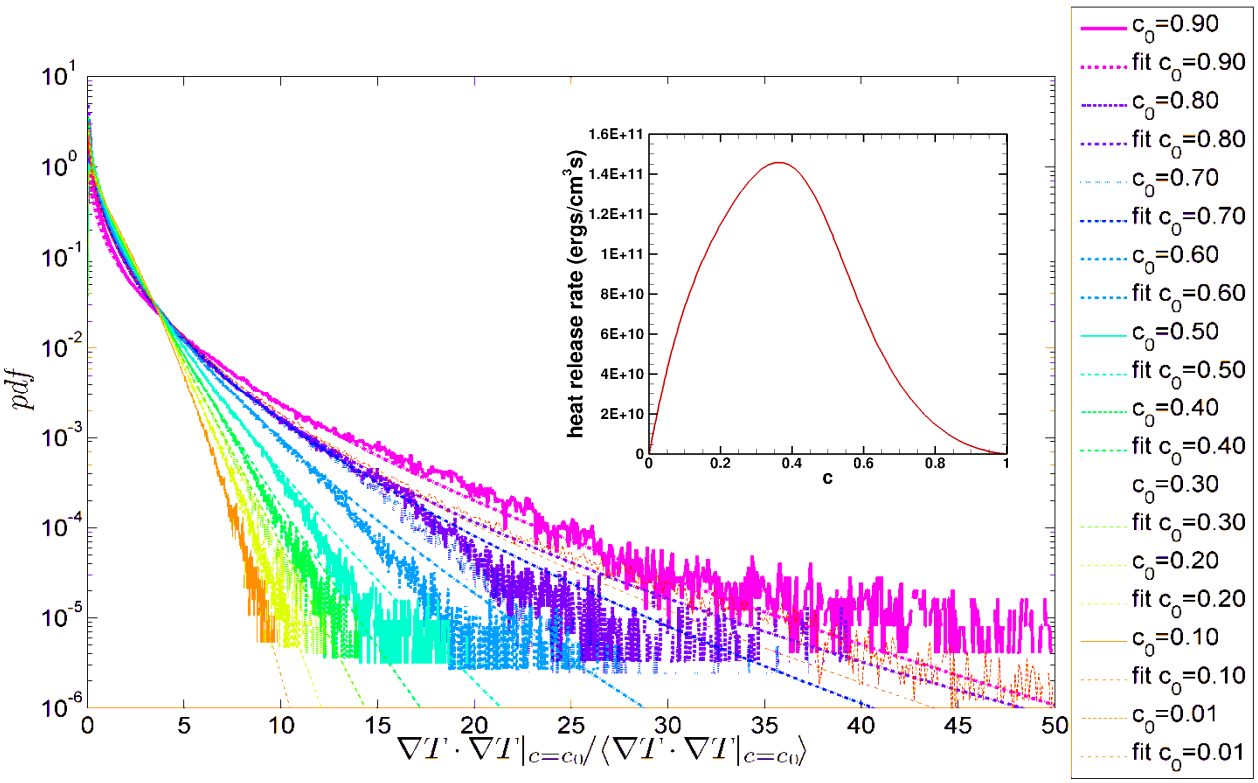

Figure 11: (a) Probability density function (pdf) of CSDR (Eq. 3) for the ***Da-*** case normalized by the corresponding average. Dotted Lines: The fitting obtained by Eq. (8). Inset showing variation of heat release rate vs. progress variable for a corresponding planar laminar premixed flame.

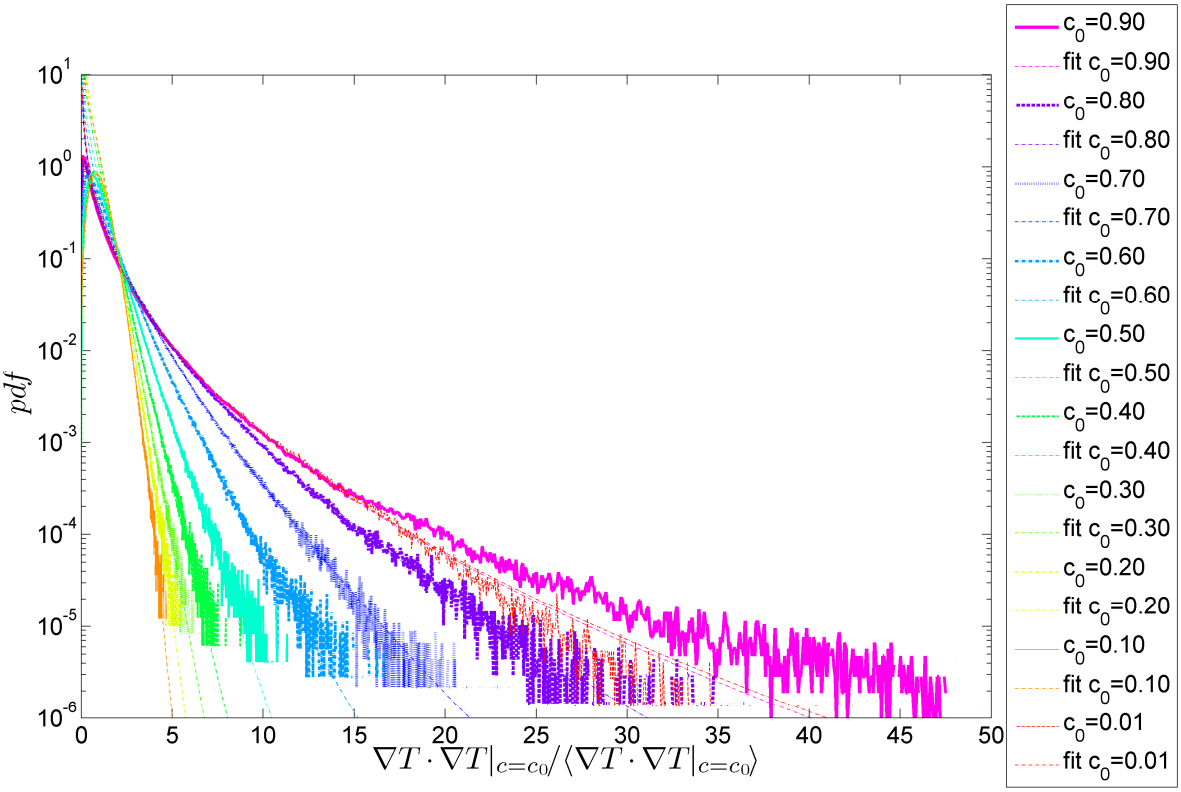

Figure 11: (b) Probability density function (pdf) of CSDR (Eq. 3) for the ***Da+*** case normalized by the corresponding average. Dotted Lines: The fitting obtained by Eq. (8)

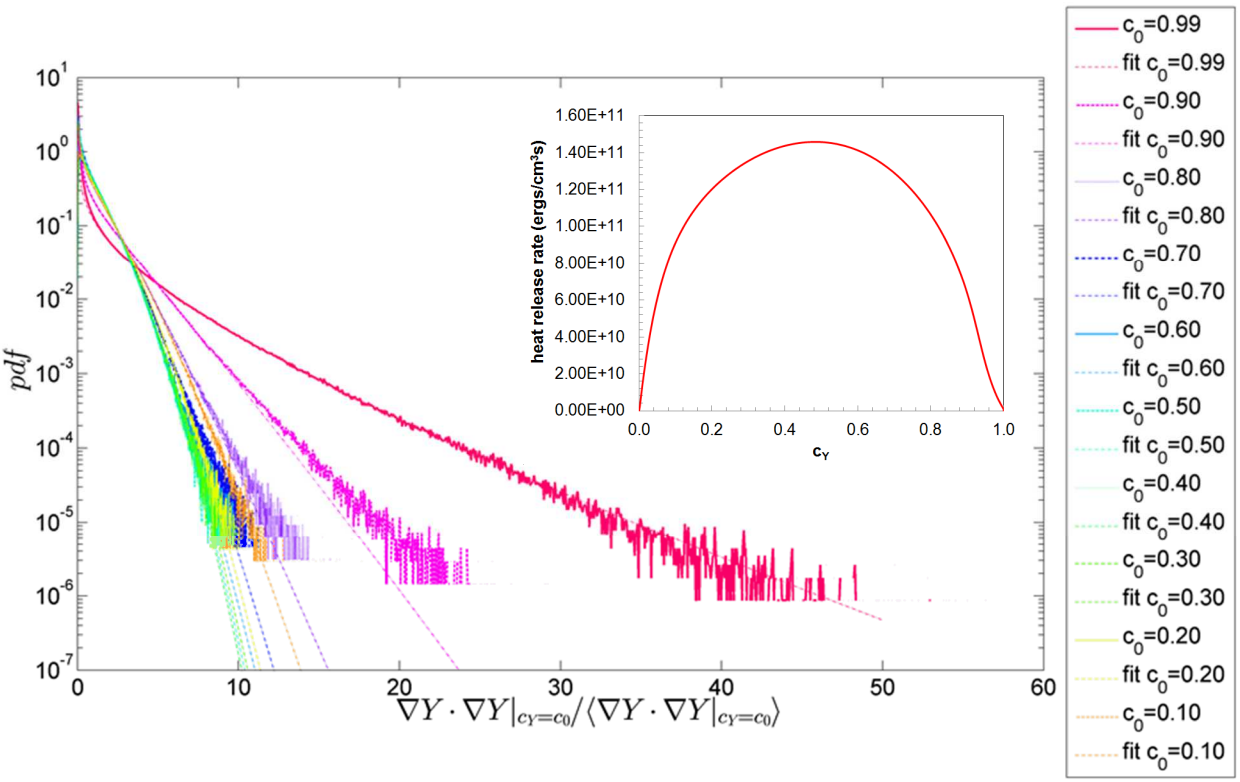

Figure 11: (c) Probability density function (pdf) of CSDR (Eq. 3) based on O_2 mass fraction gradient for the ***Da-*** case normalized by the corresponding average. Dotted Lines: The fitting obtained by Eq. (8).

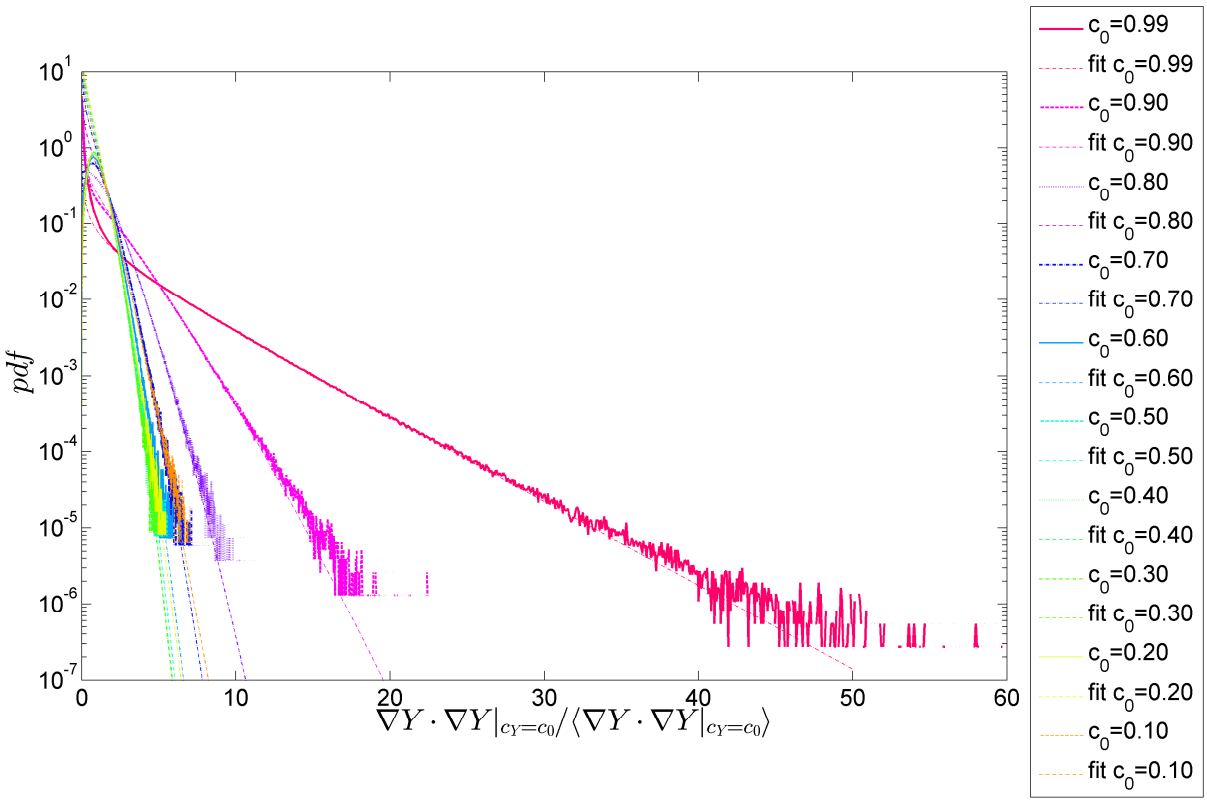

Figure 11: (d) Probability density function (pdf) of CSDR (Eq. 3) based on O_2 mass fraction gradient for the ***Da+*** case normalized by the corresponding average. Dotted Lines: The fitting obtained by Eq. (8).

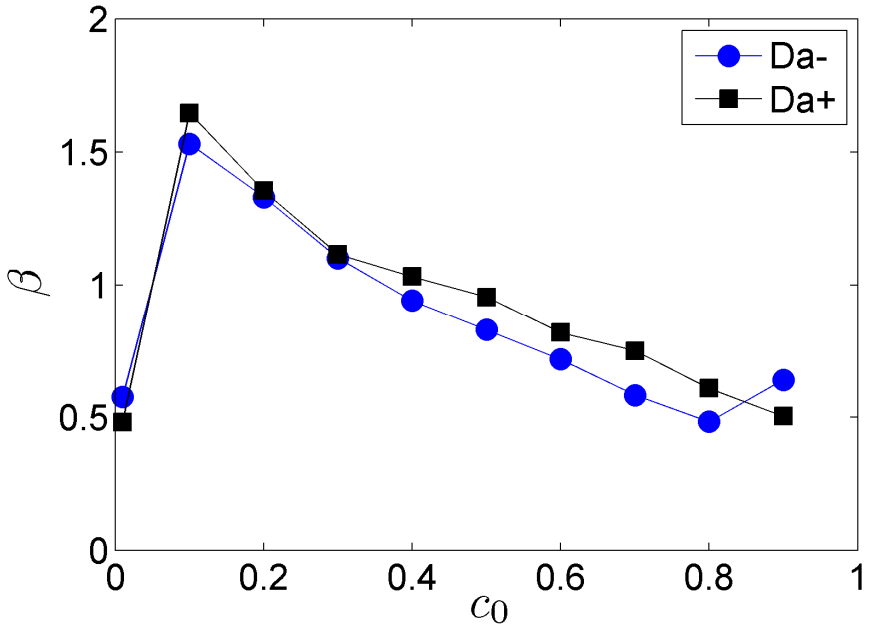

Figure 12: (a) Variation of the exponent of the stretched/compressed exponential pdf (Eq. 6) for CSDR based on temperature gradient ***Da-*** and ***Da+*** cases.

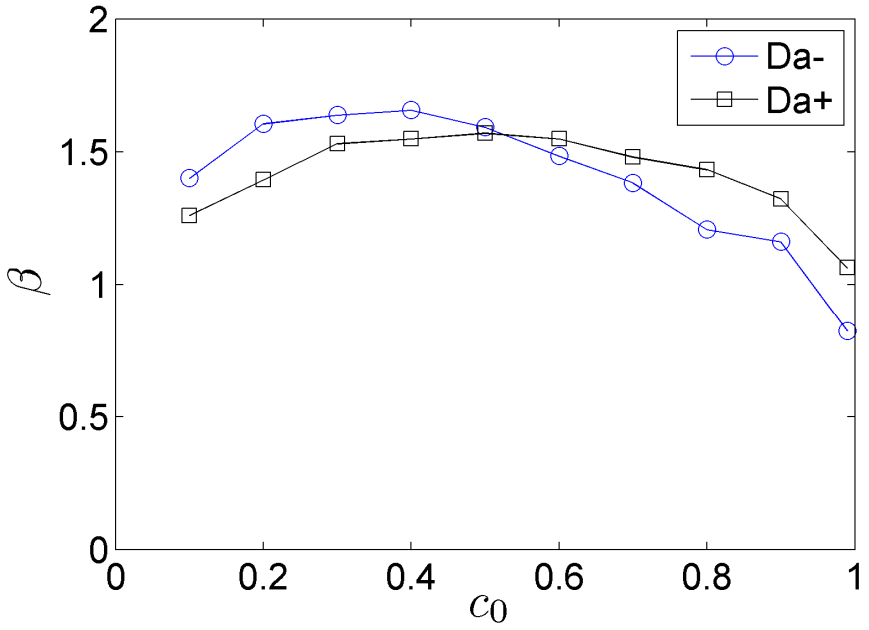

Figure 12: (b) Variation of the exponent of the stretched/compressed exponential pdf (Eq. 6) for CSDR based on O_2 mass fraction gradient ***Da-*** and ***Da+*** cases.